

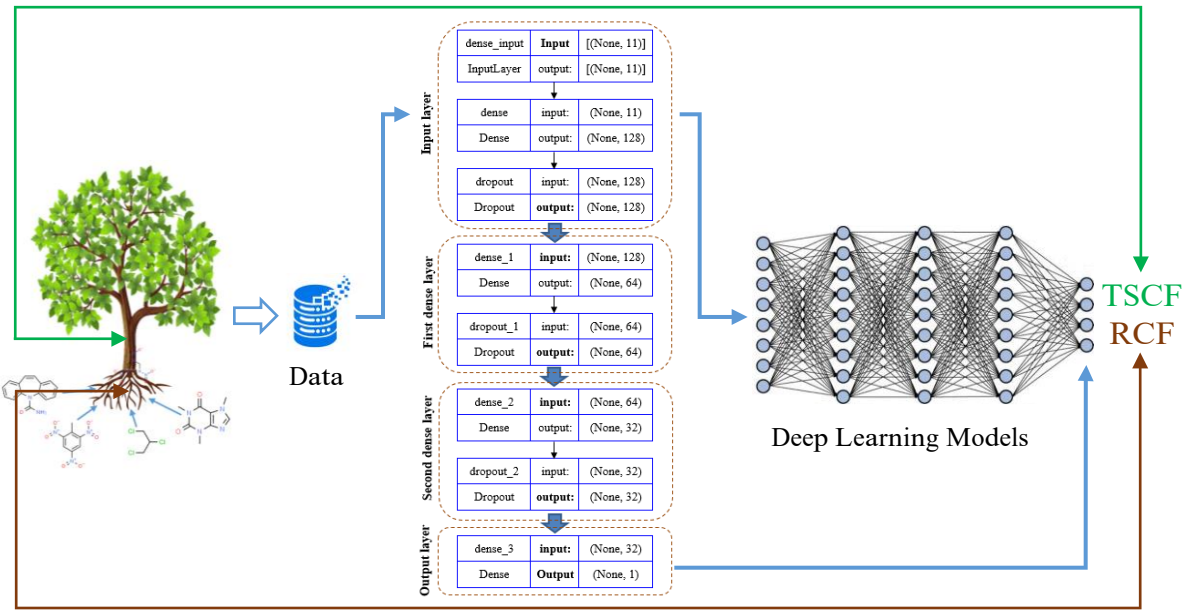
Journal of Hazardous Materials

Deep learning models for predicting plant uptake of emerging contaminants by

including the role of plant macromolecular compositions

--Manuscript Draft--

Manuscript Number:	HAZMAT-D-24-12549R1
Article Type:	Research Paper
Keywords:	Emerging contaminants; TSCF; RCF; machine learning; deep learning
Corresponding Author:	Majid Bagheri Savannah State University Savannah, UNITED STATES
First Author:	Majid Bagheri
Order of Authors:	Majid Bagheri Shai McKenney Julie Gabriella Ware Nakisa Farshforoush
Suggested Reviewers:	Amin Shams, PhD amin.shams@semnan.ac.ir Lorenzo Rossi, PhD l.rossi@ufl.edu



1
2
3
4 1 Deep learning models for predicting plant uptake of emerging contaminants by including
5 2 the role of plant macromolecular compositions
6
7
8 4 Majid Bagheri^{1,*}, Shai McKenney¹, Julie Gabriella Ware¹, Nakisa Farshforoush²
9
10 6 ¹ Department of Engineering Technology, Savannah State University, Savannah, GA 31404.
11 7 ² Department of Electrical and Computer Engineering, Tabriz University, Tabriz, Iran.
12
13
14
15 9 *Corresponding author: Majid Bagheri. Department of Engineering Technology, Savannah
16 10 State University, Savannah, GA 31404, USA.
17 11 Email: bagherim@savannahstate.edu, Phone: 912-358-3262
18
19
20
21
22 14 Abstract
23
24 15 Deep learning models can predict uptake of emerging contaminants in plants with improved
25
26 16 accuracy because they leverage advanced data-driven approaches to capture non-linear
27
28 17 relationships that traditional models struggle to address. Traditional models suffer from low
29
30 18 accuracy in predicting transpiration stream concentration factor (TSCF) and root concentration
31
32 19 factor (RCF). This study applied deep neural networks (DNN), recurrent neural networks (RNN),
33
34 20 and long short-term memory (LSTM) to enhance the accuracy of predictive models for TSCF and
35
36 21 RCF. The three models used nine chemical properties and two plant root macromolecular
37
38 22 compositions for predicting TSCF and RCF. The results indicated that deep learning models
39
40 23 predict TSCF and RCF with improved accuracy compared to mechanistic models. The coefficient
41
42 24 of determination (R^2) for the DNN, RNN, and LSTM models in predicting TSCF was 0.62, 0.67,
43
44 25 and 0.56, respectively. The corresponding mean squared error (MSE) on the test set for the models
45
46 26 was 0.055, 0.035, and 0.060, respectively. The R^2 for the DNN, RNN, and LSTM models in
47
48 27 predicting RCF was 0.90, 0.91, and 0.84, respectively. The corresponding MSE for the models
49
50 28 was 0.124, 0.071, and 0.126, respectively. The results of feature extraction using extreme gradient
51
52 29 boosting underlined the importance of lipophilicity and root lipid fraction.
53
54
55
56
57
58
59 30 Keywords: Emerging contaminants, TSCF, RCF, machine learning, deep learning.
60
61
62
63
64
65

1
2
3
4 31 1. Introduction
5
6

7 32 Predictive models aid in risk assessments, regulatory frameworks, and the formulation of
8 33 sustainable strategies for mitigating environmental and human health concerns associated with
9 34 emerging contaminants (Liu et al., 2024; Villeneuve et al., 2019). Predicting the uptake and
10 35 translocation of emerging contaminants in plants is a critical task, especially in the context of
11 36 assessing potential risks and impacts on both ecosystems and human health (Shi et al., 2022). This
12 37 research area investigates the mechanisms by which plants take up and distribute emerging
13 38 contaminants, such as pharmaceuticals and industrial chemicals, from soil or water into various
14 39 plant tissues (Bagheri et al., 2023). Understanding these processes is essential for evaluating the
15 40 bioaccumulation potential and potential transfer of contaminants along the food chain (Chormare
16 41 and Kumar, 2022; Rossi et al., 2019). The modeling of transpiration stream concentration factor
17 42 (TSCF) and root concentration factor (RCF) plays a vital role in unraveling the intricate dynamics
18 43 of plant-contaminant interactions (Trapp, 2000). The TSCF represents the ratio of the
19 44 concentrations of emerging contaminants in the plant's transpiration stream to those in the
20 45 surrounding soil (exposure media). This factor sheds light on the contaminant's mobility within
21 46 the plant and its potential transfer to other tissues (Bagheri et al., 2021). The RCF characterizes
22 47 the accumulation of contaminants in the plant roots relative to the concentration in the exposure
23 48 media (Li et al., 2022).

49 49 Uptake, translocation, and accumulation of contaminants in plants are generally encapsulated
50 50 in mathematical models that integrate factors such as plant physiology, soil characteristics, and the
51 51 physicochemical properties of chemicals (Dourado Junior et al., 2017). These mechanistic models
52 52 provide valuable insights into the fate and transport of emerging contaminants (Brunetti et al.,
53 53 2021; Trapp, 2004). Since 1974, a number of modeling studies have offered relationships between
54
55
56
57
58
59
60
61
62
63
64
65

1
2
3
4 54 the physicochemical properties of contaminants and their uptake by plants, mainly using the
5 octanol/water partition coefficient ([Briggs et al., 1982](#)). These single-parameter relationships
6
7 55 suffered from low accuracy and limited applicability for different plant species and chemical
8 compounds. Compartmental models, which take into account more physicochemical and
9 environmental properties and incorporate the complexity of uptake and translocation processes,
10
11 56 did not offer high predictive accuracy ([Collins and Finnegan, 2010](#)). The accuracy of predictions
12
13 57 for TSCF was improved by considering more physicochemical properties in a numerical modeling
14 process ([Limmer and Burken, 2014](#)).
15
16
17
18
19
20
21
22
23

24 62 The applications of artificial intelligence (AI) and machine learning (ML) models to predict
25
26 63 TSCF and RCF offered several advantages over traditional modeling approaches ([Zhong et al.,](#)
27
28 64 [2021](#)). Multi-layer perceptron neural networks significantly improved the accuracy of predictions
29
30 65 for both TSCF and RCF compared to the previous approaches. With solely relying on six
31
32 66 physicochemical properties, the multi-layer perceptron neural networks outperformed traditional
33
34 67 models and complemented the findings of previous studies in some aspects ([Bagheri et al., 2020](#)).
35
36
37 68 The fuzzy logic technique also indicated that molecular weight is a significant factor in explaining
38
39 69 the uptake efficiency of moderately hydrophobic and hydrophilic compounds ([Bagheri et al.,](#)
40
41 70 [2019](#)). In a more recent study ([Gao et al., 2022](#)), the applications of several classical ML and
42
43 71 ensemble learning algorithms resulted in improved prediction accuracy for RCFs. These ML
44
45 72 models achieved high accuracy by learning nonlinear relationships between RCFs and the
46
47 73 properties of contaminants, soils, and plants. Among ensemble learning models, gradient-boosted
48
49 74 regression trees showed higher predictive performance for the root uptake of per- and
50
51 75 polyfluoroalkyl substances, with accuracies up to 0.85 ([Xiang et al., 2023](#)).
52
53
54
55
56
57
58
59
60
61
62
63
64
65

1
2
3
4 76 The current research is an effort to improve the accuracy of predicting the TSCF and RCF by
5
6 77 applying three deep learning models. To the best of our knowledge, this is the first study that
7
8 78 employs deep neural networks (DNN), recurrent neural networks (RNN), and long short-term
9
10 79 memory (LSTM) models to predict both TSCF and RCF for emerging contaminants. The
11
12 80 predictions are based on nine chemical properties and two plant root macromolecular
13
14 81 compositions. The feature importance analysis is performed for the input variables of the models
15
16 82 using extreme gradient boosting (XGBoost). The relationship between fractions of
17
18 83 macromolecules in the plant roots and concentration factors (TSCF and RCF) for the emerging
19
20 84 contaminants is missing. The role of root macromolecular fractions in the uptake of emerging
21
22 85 contaminants is examined through feature importance analysis.

27 86
28
29
30
31 87 2. Materials and Methods
32
33
34 88 2.1. Data sets

35
36 89 Comprehensive data sets were compiled from published studies for the modeling of both
37
38 90 TSCF and RCF, see [Supplementary Material](#). The selected TSCF values included 288 records of
39
40 91 151 compounds measured in 33 plant genera under various experimental approaches from 42
41
42 92 studies. The RCF data set included 342 values for 96 compounds in 44 plant genera measured
43
44 93 under various experimental approaches from 19 studies. The inclusion of various chemicals and
45
46 94 plant species in the data sets makes it possible to develop models that are not compound- or plant-
47
48 95 specific. The data sets did not include TSCFs and RCFs from studies when there was no evidence
49
50 96 of reaching a steady state, roots were damaged, depletion of dosing solution was higher than 50%,
51
52 97 other modes of exposure were included, or calculations were not reliable ([Limmer and Burken](#),
53
54
55
56
57
58
59
60
61
62
63
64
65

1
2
3
4 98 2014). The data sets also did not include TSCFs and RCFs when the metabolism of the parent
5
6 99 compound in plants was observed or measurements included metabolites.
7
8

9 100 The data sets included nine physicochemical properties and two plant root properties. The
10
11 101 physicochemical properties were octanol/water partition coefficient (log Kow), molecular weight
12
13 102 (MW), hydrogen bond donor (HBD), hydrogen bond acceptor (HBA), rotatable bonds (RB), polar
14
15 103 surface area (PSA), vapor pressure (VP), half-life (HL), and water solubility (WS). The
16
17 104 experimental values of the properties were considered in the analyses when both predicted and
18
19 105 experimental values were available. The chemical properties were obtained from chemical
20
21 106 structure databases, including the US EPA Chemistry Dashboard and ChemSpider. The two plant
22
23 107 root properties were fractions of the lipids and proteins in the roots. The macromolecular
24
25 108 composition of the plant roots was obtained from published studies. [Table 1](#) represents a summary
26
27 109 of the chemical and plant root properties used for developing deep learning models for both TSCF
28
29 110 and RCF.
30
31
32
33
34 111
35
36 112 2.2. Pattern recognition analysis
37
38
39 113 t-distributed stochastic neighbor embedding (t-SNE) was used for exploratory data analysis
40
41 114 and to detect important patterns in the data sets. t-SNE involves a dimensionality reduction method
42
43 115 to reveal and visualize patterns within complex data sets ([Zhu et al., 2019](#)). It focuses on preserving
44
45 116 local relationships and capturing the intrinsic structure of the data. t-SNE is particularly effective
46
47 117 for identifying clusters that might be challenging to discern in the high-dimensional spaces of plant
48
49 118 uptake problems ([Kim et al., 2023](#)). This technique facilitates the visualization of intricate patterns
50
51 119 and clusters within the TSCF and RCF data sets by mapping data points to a lower-dimensional
52
53 120 space. However, t-SNE preserves pairwise similarities between the high-dimensional spaces.
54
55
56
57
58
59
60
61
62
63
64
65

1
2
3
4 121 2.3. Feature importance analysis
5
6 122 Feature importance analysis is an ML approach for examining the contribution of each input
7
8 123 parameter to the predictive models (Zien et al., 2009). It particularly helps determine which
9
10 124 parameters have the most influence on the prediction of TSCF and RCF. In this study, XGBoost
11
12 125 was used to analyze the importance of the nine physiochemical and two plant root properties for
13
14 126 the modeling processes. Feature extraction in XGBoost often refers to the importance scores
15
16 127 assigned to each feature during the training process. XGBoost assigns weights to features based
17
18 128 on their contribution to predictive accuracy (Wade and Glynn, 2020). These importance scores
19
20 129 quantify the influence of each input parameter of the models in making predictions for the TSCF
21
22 130 and RCF. The XGBoost models were developed using scikit-learn, which is an ML library in
23
24 131 Python (Hackeling, 2017). Each data set was divided into 80% for training and 20% for testing the
25
26 132 models. Both data sets were rescaled using StandardScaler to have a standard normal distribution
27
28 133 with a mean of 0 and a standard deviation of 1. The hyperparameters of the XGBoost models were
29
30 134 optimized through randomized search cross-validation (Bergstra and Bengio, 2012). The XGBoost
31
32 135 models showed the highest performance, with a maximum depth of 4 and a learning rate of 0.15.
33
34 136
35
36 137 2.4. Deep learning model training
37
38 138 Three deep learning models, including DNN, RNN, and LSTM, were applied to predict TSCF
39
40 139 and RCF. The models were designed and developed in Python using TensorFlow, which is an
41
42 140 open-source machine learning library (Ramsundar and Zadeh, 2018). For the three deep learning
43
44 141 models, 80% of the data was used for training and 20% for testing. The data was rescaled using
45
46 142 StandardScaler to have a standard normal distribution before training. Optimized hyperparameters
47
48 143 for the three deep learning models were achieved through randomized search cross-validation.
49
50
51
52
53
54
55
56
57
58
59
60
61
62
63
64
65

1
2
3
4 144 The DNN models are neural networks with multiple layers, typically including an input layer,
5
6 145 one or more hidden layers, and an output layer. The DNN for predicting TSCF and RCF had two
7
8 146 hidden layers. The architecture of the DNN model with eleven input variables for predicting TSCF
9
10 147 and RCF is shown in [Fig. 1](#). The input layer, first hidden layer, and second layer had 128, 64, and
11
12 148 32 computational neurons, respectively. A dropout of 0.2 was implemented after input and hidden
13
14 149 layers to make the predictions reliable. During the training steps, the network adjusts its weights
15
16 150 and biases through a backpropagation, minimizing the difference between predicted and measured
17
18 151 outputs ([Zhu et al., 2018](#)). Adaptive moment (Adam), which is a replacement optimization
19
20 152 algorithm for stochastic gradient descent, was used as the optimizer of the DNN models. Each
21
22 153 layer of the DNN performs computations on the input data and transforms it into abstract
23
24 154 representations. Activation functions apply non-linearity and enable the network to capture
25
26 155 relationships within the data ([Ding et al., 2018](#)). The activation function of the input and hidden
27
28 156 layers of the DNN models was a rectified linear unit (ReLU). Through multiple iterations of
29
30 157 training on the measured data, a well-trained DNN can generalize its learned features to make
31
32 158 accurate predictions on new test data ([Larochelle et al., 2009](#)). The depth and complexity of DNN
33
34 159 models allow them to automatically extract important features, which in turn makes them highly
35
36 160 effective in predicting plant uptake.

45
46 161 Deep RNN models are neural networks that handle sequential data by incorporating memory
47
48 162 mechanisms. It consists of multiple layers of interconnected computational neurons, each
49
50 163 processing information over time ([Kanagachidambaresan et al., 2021](#)). In this study, the RNN
51
52 164 models had one input layer and two hidden layers with 150 computational neurons. Unlike
53
54 165 traditional feedforward neural networks, deep RNN models have connections that form directed
55
56 166 cycles. This allows them to maintain a memory of previous inputs and leverage temporal
57
58 167
59
60
61
62
63
64
65

1
2
3
4 167 information for prediction. For training the RNN models, the network is iteratively exposed to
5
6 sequential input data. The network adjusts its internal parameters to minimize the discrepancy
7
8 168 between predicted and measured outputs (Sutskever, 2013). The weights and biases of the RNN
9
10 models were adjusted using adaptive moment estimation. Similar to the DNNs, the activation
11
12 170 function of the input and hidden layers of the RNN models was a rectified linear unit.
13
14 171
15
16 172 The LSTM models are RNNs that capture long-term dependencies in sequential data and
17
18 address vanishing gradient problems (Sherstinsky, 2020). During training, LSTMs utilize
19
20 backpropagation through time to compute gradients and adjust the weights. The activation
21
22 174 functions play a crucial role in information flow and memory cell modulation. LSTMs introduce
23
24 175 memory cells with self-regulating mechanisms, including input, forget, and output gates. The input
25
26 176 gate determines which information is stored, the forget gate regulates what information is
27
28 177 discarded, and the output gate decides what information is passed to the next time step (Manaswi
29
30
31 178 and Manaswi, 2018). This architecture enables LSTM models to selectively retain or forget
32
33 179 information over long sequences and allows them to capture and remember relevant patterns. The
34
35 180 LSTM models for predicting TSCF and RCF had an input layer and two hidden layers with 40
36
37 181 computational neurons in the optimal conditions. The activation function of the input and hidden
38
39 182 layers was a rectified linear unit. The adaptive moment estimation outperformed other methods in
40
41 183 adjusting the weights and biases.
42
43
44
45
46 184
47
48 185
49
50
51 186 2.5. Performance evaluation
52
53 187 Evaluating the performance of deep learning models is a critical step in assessing the
54
55 effectiveness and reliability of their predictions. Mean squared error (MSE), which is a common
56
57 188 loss function in regression problems, was used to measure the average squared difference between
58
59
60
61
62
63
64
65

1
2
3
4 190 predicted values and actual values. The lower values of MSE indicate better performance. The
5
6 191 coefficient of determination (R-squared or R^2) was used to evaluate the goodness of fit of
7
8 192 regression models. The MSE and R^2 are calculated as follow:
9
10

11 193
$$MSE = 1/n \sum_{i=1}^n (y_{pi} - y_{ti})^2 \quad (1)$$

12 194
$$R^2 = 1 - \sum_{i=1}^n (y_{ti} - y_{pi})^2 / \sum_{i=1}^n (y_{ti} - \bar{y})^2 \quad (2)$$

13 195 where \bar{y} is the average of y over the n data, y_t is the actual value, and y_p is the predicted value.
14
15

16 196 The performance of XGBoost for the feature importance analysis was examined based on the
17 197 F1 score. The F1 score combines precision and recall into a single metric, considering both false
18
19 198 positives and false negatives of the predictions. The F1 is calculated as follow:
20
21

22 199
$$F1 \text{ score} = TP / (TP + 1/2(FP + FN)) \quad (3)$$

23 200 where TP is true positive, FP is false positive, and FN is false negative.
24
25

26 201
27
28 202 2.6. Plant macromolecular compositions
29
30

31 203 Chemicals either accumulate in the roots or cross the plant root membranes and transport to
32
33 204 the upper tissues through the vascular pathways. Plant roots and shoots are composed of water,
34
35 205 wax, lignin, cellulose, lipids, phenolics, and non-structural carbohydrates ([Gupta and Singh, 1981](#)).
36
37

38 206 While lipophilicity is an important factor, predicting the uptake of emerging contaminants solely
39
40 207 based on lipids is a simplified approach. The fraction of root macromolecules such as protein is
41
42 208 not negligible since these materials (protein, lignin, and cellulose) were shown to be important in
43
44 209 other biological systems ([Endo et al., 2012](#); [Jonker, 2008](#); [Stoklosa et al., 2013](#)). It is assumed that
45
46 210 the partitioning of emerging contaminants into plant roots and other tissues is equal to the
47
48 211 partitioning of compounds into macromolecules. In this study, the changes in concentration
49
50 212 factors, including TSCF and RCF, will be examined over a wide range of root macromolecular
51
52
53
54
55
56
57
58
59
60
61
62
63
64
65

1
2
3
4 213 fractions. The results of feature extraction will be used to analyze the uptake and translocation of
5
6 214 emerging contaminants based on the fractions of lipids and proteins in the roots.
7
8
9 215
10
11
12 216 3. Results and Discussion
13
14 217 3.1. Hidden patterns in the data
15
16 218 The results of pattern recognition using t-SNE to visualize the possible clusters in the TSCF
17
18 219 and RCF data sets are shown in [Fig. 2](#). The first dimension is derived in such a way that similar
20
21 220 data points in the original space are also close to each other in this new dimension. Similarly, the
22
23 221 second dimension is also obtained by preserving pairwise similarities between data points. The
24
25 222 results for both TSCF and RCF showed different clusters in the data sets. For the RCF, the clusters
26
27 223 for the compounds with the higher root concentration factors formed separate clusters. The
28
29 224 perfluoroalkyl family of chemicals was found to have higher RCFs, as shown in the separate
30
31 225 clusters in [Fig. 2](#). The observations of another study also indicated that the clusters in the RCF data
32
33 226 reflect the similarities across different combinations of chemicals, plants, and soils ([Gao et al.,](#)
34
35 227 [2022](#)). For the TSCF, the clusters are less distinguishable compared to the RCF data. However,
36
37 228 the plant species and compounds with higher uptake efficiency were clustered closer. This is in
38
39 229 line with the results of a previous study, which stated that tomato is a species with higher uptake
40
41 229 potential ([Bagheri et al., 2019](#)).
42
43
44
45
46
47
48
49
50
51 231
52
53 232 3.2. Significant features for predicting TSCF and RCF
54
55
56 233 The feature importance analysis using XGBoost based on nine physicochemical properties
57
58 234 and two plant root properties yielded insightful findings ([Fig. 3](#)). The octanol/water partition
59
60 235 coefficient (log Kow) and molecular weight (MW) were two paramount predictors for both TSCF
61
62
63
64
65

1
2
3
4 236 and RCF, as reflected by their high F1 scores. Particularly, the log Kow, with F1 scores of 209 and
5
6 237 215 for TSCF and RCF, respectively, emphasized its critical role in predicting these concentration
7
8 238 factors. The F1 scores of the MW for predicting TSCF and RCF were 167 and 131. Previous
9
10 239 studies using statistical methods such as stepwise regression also demonstrate that log Kow and
11
12 239 MW are significant variables in the prediction of both TSCF and RCF (Bagheri et al., 2020;
13
14 240 Bagheri et al., 2019). The feature importance analysis using XGBoost also showed that lipid and
15
16 241 protein fractions are other significant predictors, with high F1 scores for both variables. The lipid
17
18 242 fraction with high F1 scores of 189 and 187 for the TSCF and RCF models was the second
19
20 243 significant predictor. The feature importance analyses using neural networks and regression trees
21
22 244 also indicated the lipid fraction as a major predictor for the RCF (Gao et al., 2022). The protein
23
24 245 fraction of the plant roots, with high F1 scores of 126 and 100 for the TSCF and RCF, was found
25
26 246 to be another significant predictive feature. Despite their importance, the role of proteins and
27
28 247 macromolecules other than lipids in the uptake and translocation of emerging contaminants in
29
30 248 plants has never been deeply studied. These results underscore the importance of understanding
31
32 249 the interactions between chemical and root properties in plant uptake modeling and provide
33
34 250 valuable insights for risk assessments and ecological management strategies.
35
36 251
37
38 252
39
40
41
42
43
44
45
46 253 3.3. Predictive models for TSCF
47
48 254 The three deep learning models showed improved accuracy on the test data sets for the
49
50 255 prediction of TSCF. The results indicated that deep RNN models have the highest performance
51
52 256 based on R-squared and MSE values (Fig. 4). The deep RNN achieved the highest accuracy with
53
54 257 an R^2 of 0.67 and an MSE of 0.35. The training history based on train and test data sets indicated
55
56 258 that the RNN models are reliable without any overfitting or underfitting. The close values for the
57
58
59
60
61
62
63
64
65

1
2
3
4 259 train and test losses confirm the reliability of the predictions by the RNN models. The performance
5
6 260 of the RNN models based on the tests was positive compared to the traditional models and simple
7
8 261 neural networks, with MSEs of 0.25 and 0.037, respectively (Bagheri et al., 2019; Doucette et al.,
9
10 262 2018; Schriever and Lamshoeft, 2020). Despite the high accuracy of the simple neural networks,
11
12 263 their predictive performance was not consistent for different compounds since the models did not
13
14 264 consider important chemical and plant properties (Bagheri et al., 2019). The RNN models were
15
16 265 followed by DNNs with an R^2 of 0.62 and an MSE of 0.55. The training history for the DNN
17
18 266 models showed that train and test losses are close over 100 epochs. The LSTM model predicted
19
20 267 the TSCF with lower accuracy compared to the RNN and DNN models. The best values of R^2 and
21
22 268 MSE on the test data set for the LSTM models were 0.56 and 0.06, respectively.
23
24
25
26
27

28 269 The results of this study demonstrated the importance and need for considering plant
29
30 270 properties in the modeling of plant uptake. The macromolecular compositions were significant and
31
32 271 relevant parameters for the prediction of concentration factors. One of the main drawbacks of the
33
34 272 single-parameter models based on lipophilicity was their applicability to specific chemicals or
35
36 273 plant species (Limmer and Burken, 2014). The models considered fractions of lipids and proteins
37
38 274 in the plant roots, which in turn make the models applicable for different plant species. The model
39
40 275 also considered vapor pressure and biodegradation half-lives for the chemicals as two new input
41
42 276 parameters. These chemical properties improved the reliability of the predictive models,
43
44 277 particularly for volatile and degradable compounds. The feature importance analysis showed that
45
46 278 these properties are important since they had relatively high F1 scores. The vapor pressure had F1
47
48 279 scores of 105 and 114, and the biodegradation half-lives had F1 scores of 100 and 51 for the TSCF
49
50 280 and RCF.
51
52
53
54
55
56
57
58 281
59
60
61
62
63
64
65

1
2
3
4 282 3.4. Predictive models for RCF
5
6
7 283 The deep learning algorithms predicted the RCF with higher performance compared to the
8
9 284 TSCF. The three deep learning models outperformed previous traditional and data-driven models
10
11 285 for predicting the RCF. The three deep learning models predicted the logarithm of the RCF for
12
13 286 better visualization representation. Similar to the results for the TSCF, the deep RNN models
14
15 287 indicated the highest performance for the prediction of the RCF (Fig. 5). The deep RNN achieved
16
17 288 the highest accuracy with an R^2 of 0.91 and an MSE of 0.071. This model was followed by the
18
19 289 DNN with an R^2 of 0.9 and an MSE of 0.124. The training of the RNN and DNN models was
20
21 290 successful, as shown by the decreasing losses of the train and test data sets. The close and
22
23 291 decreasing losses for train and test sets proved the lack of overfitting or underfitting in both deep
24
25 292 learning models. The RNN and DNN models showed significant improvement over the traditional
26
27 293 single-parameter relationships with low accuracy and specificity for limited compounds (Briggs
28
29 294 et al., 1982; Chen et al., 1989). These deep learning models indicated a higher accuracy for the
30
31 295 prediction of the RCF than simple neural networks, with an R-squared of 0.82 (Bagheri et al.,
32
33 296 2020). The prediction of the log RCF using fully connected neural networks and by considering
34
35 297 different chemical and plant properties achieved an accuracy of 0.79 and a mean average error of
36
37 298 0.22 (Gao et al., 2022). In this study, even the LSTM models with an R^2 of 0.84 and an MSE of
38
39 299 0.126 showed higher performance compared to these neural network models (Fig. 5). The results
40
41 300 of this study indicated that the three deep learning models outperformed traditional and classical
42
43 301 machine learning models in predicting the TSCF and RCF (Table 2).
44
45
46
47
48
49
50
51
52
53
54
55
56
57
58
59
60
61
62
63
64
65

1
2
3
4 305 3.5. Plant uptake and root macromolecular fractions
5
6
7 306 The feature importance analyses and previous studies have emphasized the role of
8
9 307 macromolecules in plant uptake of emerging contaminants. Correlation analysis was performed to
10
11 308 examine the roles of fractions of root macromolecules in the accumulation and distribution of
12
13 309 emerging contaminants in plants. [Fig. 6](#) demonstrates the correlation of fractions of the lipids and
14
15 310 proteins in the plant roots with the log RCF. The results of this study indicated that RCFs for the
16
17 311 emerging contaminants correlate negatively with the root lipids ($P < 0.05$) and positively with the
18
19 312 root proteins ($P < 0.05$). The result for the lipids is supported by the generally accepted
20
21 313 understanding that compounds with higher lipophilicity have higher TSCFs and lower RCFs
22
23
24 314 ([Burken and Schnoor, 1998](#); [Dettenmaier et al., 2009](#)). The results of a study on the uptake and
25
26 315 accumulation of perfluorooctane sulfonate and perfluorooctanoate emphasized the importance of
27
28 316 both lipids and proteins ([Wen et al., 2016](#)). The results indicated that the perfluorooctane sulfonate
29
30 317 and perfluorooctanoate accumulations in roots correlate positively with root protein contents and
31
32 318 negatively with root lipid contents.
33
34
35
36
37
38
39 319
40
41 320 4. Conclusions
42
43
44 321 This study employed deep neural networks (DNN), recurrent neural networks (RNN), and
45
46 322 long short-term memory (LSTM) models to enhance the predictive accuracy of TSCF and RCF.
47
48
49 323 The findings demonstrated significant improvements in the predictive accuracy of these deep
50
51 324 learning models compared to the traditional models. DNN showed the highest accuracy in
52
53 325 predicting the TSCF and FCF with coefficients of determination equal to 0.67 and 0.91,
54
55 326 respectively. The mean squared error for TSCF and FCF was 0.035 and 0.071, respectively. The
56
57 327 findings of this study underscore the potential of deep learning techniques to improve predictive
58
59
60
61
62
63
64
65

1
2
3
4 328 models for plant uptake and translocation of emerging contaminants. This study also indicated the
5
6
7 329 importance of physicochemical properties and fractions of macromolecules for reliable prediction
8
9 330 of the TSCF and RCF. Including important physicochemical properties such as degradation and
10
11 331 fractions of macromolecules such as lipids and proteins in the modeling process enhanced the
12
13
14 332 reliability of predictions.
15
16 333
17 334
18
19 335 Declaration of Competing Interest
20
21 336 The authors declare that they have no competing financial interests or personal relationships
22
23
24 337 that could have appeared to influence the work reported in this paper.
25
26 338
27
28
29 339 Data Statement
30
31 340 The data for this study is available in Excel format as Supplementary Material.
32
33
34 341
35
36 342 Acknowledgments
37
38 343 The authors declare that they have no competing interests. This work was supported
39
40
41 344 by National Science Foundation under Award Number 2300369 and National Science
42
43 345 Foundation under Award Number 2348805.
44
45
46 346
47 347
48 348
49 349 References
50
51 350 Bagheri, M., Al-Jabery, K., Wunsch, D., Burken, J.G., 2020. Examining plant uptake and translocation of
52 emerging contaminants using machine learning: Implications to food security. *Sci. Total Environ.* 698, 352
53 133999. <https://doi.org/10.1016/j.scitotenv.2019.133999>
54
55 353 Bagheri, M., Al-Jabery, K., Wunsch, D.C., Burken, J.G., 2019. A deeper look at plant uptake of 354
56 environmental contaminants using intelligent approaches. *Sci. Total Environ.* 651, 561-569. 355
57 <https://doi.org/10.1016/j.scitotenv.2018.09.048>
58
59 356 Bagheri, M., He, X., Al-Lami, M.K., Oustriere, N., Liu, W., Limmer, M.A., Shi, H., Burken, J.G., 2023.
60 357 Assessing plant uptake of organic contaminants by food crops tomato, wheat, and corn through sap
61
62
63
64
65

1
2
3
4 358 concentration factor. Int. J. Phytoremediat. 25(9), 1215-1224.
5 359 <https://doi.org/10.1080/15226514.2022.2144797>
6
7 360 Bagheri, M., He, X., Oustriere, N., Liu, W., Shi, H., Limmer, M.A., Burken, J.G., 2021. Investigating plant
8 361 uptake of organic contaminants through transpiration stream concentration factor and neural network 362
9 models. *Sci. Total Environ.* 751, 141418. <https://doi.org/10.1016/j.scitotenv.2020.141418>
10
11 363 Bergstra, J., Bengio, Y., 2012. Random search for hyper-parameter optimization. *J. Mach. Learn. Res.*
12 364 13(2), 281-305.
13
14 365 Briggs, G.G., Bromilow, R.H., Evans, A.A., 1982. Relationships between lipophilicity and root uptake and
15 366 translocation of non-ionised chemicals by barley. *Pestic. Sci.* 13(5), 495-504.
16 367 <https://doi.org/10.1002/ps.2780130506>
17
18 368 Brunetti, G., Kodes' ová , R., Š vecová , H., Fér, M., Nikodem, A., Klement, A., Grabic, R., Š imu' nek, J.í.,
19 369 2021. On the use of mechanistic soil-plant uptake models: a comprehensive experimental and numerical 370
20 analysis on the translocation of carbamazepine in green pea plants. *Environ. Sci. Technol.* 55(5), 2991-371
21 3000. <https://dx.doi.org/10.1021/acs.est.0c07420?ref=pdf>
22
23 372 Burken, J.G., Schnoor, J.L., 1998. Predictive relationships for uptake of organic contaminants by hybrid
24 373 poplar trees. *Environ. Sci. Technol.* 32(21), 3379-3385.
25
26 374 Chen, Q., Briggs, G., Evans, A., 1989. Relationships between lipophilicity and root uptake and translocation
27 375 of non-ionised chemicals by rice. *Acta Agric. Nucleatae Sinica* 3, 1-3.
28
29 376 Chormare, R., Kumar, M.A., 2022. Environmental health and risk assessment metrics with special mention
30 377 to biotransfer, bioaccumulation and biomagnification of environmental pollutants. *Chemosphere* 302, 378
31 134836. <https://doi.org/10.1016/j.chemosphere.2022.134836>
32
33 379 Collins, C.D., Finnegan, E., 2010. Modeling the plant uptake of organic chemicals, including the soil- air-
34 380 plant pathway. *Environ. Sci. Technol.* 44(3), 998-1003.
35
36 381 Dettenmaier, E.M., Doucette, W.J., Bugbee, B., 2009. Chemical hydrophobicity and uptake by plant roots.
37 382 *Environ. Sci. Technol.* 43(2), 324-329.
38
39 383 Ding, B., Qian, H., Zhou, J., 2018. Activation functions and their characteristics in deep neural networks,
40 384 2018 Chin. Control Decis. Conf. IEEE, pp. 1836-1841. <https://doi.org/10.1109/CCDC.2018.8407425>
41
42 385 Doucette, W.J., Shunthirasingham, C., Dettenmaier, E.M., Zaleski, R.T., Fantke, P., Arnot, J.A., 2018. A
43 386 review of measured bioaccumulation data on terrestrial plants for organic chemicals: metrics, variability,
44 387 and the need for standardized measurement protocols. *Environ. Toxicol. Chem.* 37(1), 21-33. 388
<https://doi.org/10.1002/etc.3992>
45
46 389 Dourado Junior, S., Nunes, E., Marques, R., Rossino, L., Quites, F., Siqueira, J., Moreto, J., 2017. 390
47 Controlled release behavior of sulfentrazone herbicide encapsulated in Ca-ALG microparticles: 391
48 preparation, characterization, mathematical modeling and release tests in field trial weed control. *J. 392
49 Mater. Sci.* 52, 9491-9507. <https://doi.org/10.1007/s10853-017-1103-9>
50
51 393 Endo, S., Bauerfeind, J., Goss, K.-U., 2012. Partitioning of neutral organic compounds to structural
52 394 proteins. *Environ. Sci. Technol.* 46(22), 12697-12703. <https://doi.org/10.1021/es303379y>
53
54 395 Gao, F., Shen, Y., Sallach, J.B., Li, H., Zhang, W., Li, Y., Liu, C., 2022. Predicting crop root concentration
55 396 factors of organic contaminants with machine learning models. *J. Hazard. Mater.* 424, 127437. 397
<https://doi.org/10.1016/j.jhazmat.2021.127437>
56
57 398 Gupta, S., Singh, J., 1981. The effect of plant species, weather variables and chemical composition of plant
58 399 material on decomposition in a tropical grassland. *Plant and Soil* 59(1), 99-117.
59 400 <https://doi.org/10.1007/BF02183596>
60
61
62
63
64
65

1
2
3
4 401 Hackeling, G., 2017. Mastering Machine Learning with scikit-learn. Packt Publishing Ltd. Birmingham,
5 402 UK.
6
7 403 Jonker, M.T., 2008. Absorption of polycyclic aromatic hydrocarbons to cellulose. *Chemosphere* 70(5), 778-
8 404 782. <https://doi.org/10.1016/j.chemosphere.2007.07.020>
9
10 405 Kanagachidambaresan, G., Ruwali, A., Banerjee, D., Prakash, K.B., 2021. Recurrent neural network, in:
11 406 Prakash, K.B., Kanagachidambaresan, G. R. (Eds.), *Programming with TensorFlow: Solution for Edge* 407
12 Computing Applications, Springer Cham, Ghent, Belgium, pp. 53-61. https://doi.org/10.1007/978-3-408-030-57077-4_7
13
14 409 Kim, J., Lee, C., Park, J., Kim, N., Kim, S.-L., Baek, J., Chung, Y.-S., Kim, K., 2023. Comparison of 410
15 Various Drought Resistance Traits in Soybean (*Glycine max* L.) Based on Image Analysis for Precision 411
16 Agriculture. *Plants* 12(12), 2331. <https://doi.org/10.3390/plants12122331>
17
18 412 Larochelle, H., Bengio, Y., Louradour, J., Lamblin, P., 2009. Exploring strategies for training deep neural
19 413 networks. *J. Mach. Learn. Res.* 10(1).
20
21 414 Li, Y., Sallach, J.B., Zhang, W., Boyd, S.A., Li, H., 2022. Characterization of plant accumulation of 415
22 pharmaceuticals from soils with their concentration in soil pore water. *Environ. Sci. Technol.* 56(13), 416
23 9346-9355. <https://doi.org/10.1021/acs.est.2c00303>
24
25 417 Limmer, M.A., Burken, J.G., 2014. Plant translocation of organic compounds: molecular and 418
26 physicochemical predictors. *Environ. Sci. Technol. Lett.* 1(2), 156-161.
27 419 <https://doi.org/10.1021/ez400214q>
28
29 420 Liu, S., Qiu, Y., He, Z., Shi, C., Xing, B., Wu, F., 2024. Microplastic-derived dissolved organic matter and
30 421 its biogeochemical behaviors in aquatic environments: A review. *Crit. Rev. Environ. Sci. Technol.* 422
31 54(11), 865-882. <https://doi.org/10.1080/10643389.2024.2303294>
32
33 423 Manaswi, N.K., 2018. RNN and LSTM, in: Manaswi, N.K. (Eds.), *Deep Learning with Applications Using*
34 424 *Python: Chatbots and Face, Object, and Speech Recognition With TensorFlow and Keras*. Springer, 425
35 Berkeley, CA, pp. 115-126. https://doi.org/10.1007/978-1-4842-3516-4_9
36
37 426 Ramsundar, B., Zadeh, R.B., 2018. *TensorFlow for deep learning: from linear regression to reinforcement*
38 427 *learning*. " O'Reilly Media, Inc.", Sebastopol, CA.
39
40 428 Rossi, L., Bagheri, M., Zhang, W., Chen, Z., Burken, J.G., Ma, X., 2019. Using artificial neural network to
41 429 investigate physiological changes and cerium oxide nanoparticles and cadmium uptake by *Brassica* 430
42 napus plants. *Environ. Pollut.* 246, 381-389. <https://doi.org/10.1016/j.envpol.2018.12.029>
43
44 431 Schriever, C., Lamshoeft, M., 2020. Lipophilicity matters—a new look at experimental plant uptake data
45 432 from literature. *Sci. Total Environ.* 713, 136667. <https://doi.org/10.1016/j.scitotenv.2020.136667>
46
47 433 Sherstinsky, A., 2020. Fundamentals of recurrent neural network (RNN) and long short-term memory
48 434 (LSTM) network. *Physica D: Nonlinear Phenom.* 404, 132306.
49 435 <https://doi.org/10.1016/j.physd.2019.132306>
50
51 436 Shi, Q., Xiong, Y., Kaur, P., Sy, N.D., Gan, J., 2022. Contaminants of emerging concerns in recycled water:
52 437 Fate and risks in agroecosystems. *Sci. Total Environ.* 814, 152527.
53 438 <https://doi.org/10.1016/j.scitotenv.2021.152527>
54
55 439 Stoklosa, R.J., Velez, J., Kelkar, S., Saffron, C.M., Thies, M.C., Hodge, D.B., 2013. Correlating lignin
56 440 structural features to phase partitioning behavior in a novel aqueous fractionation of softwood Kraft 441
57 black liquor. *Green Chem.* 15(10), 2904-2912. <https://doi.org/10.1039/C3GC41182F>
58
59 442 Sutskever, I., 2013. Training recurrent neural networks. University of Toronto, Toronto, ON, Canada.
60
61
62
63
64
65

1
2
3
4 443 Trapp, S., 2000. Modelling uptake into roots and subsequent translocation of neutral and ionisable organic
5 444 compounds. Pest Manag. Sci. 56(9), 767-778. [https://doi.org/10.1002/1526-4998\(200009\)56:9%3C767::AID-PS198%3E3.0.CO;2-Q](https://doi.org/10.1002/1526-4998(200009)56:9%3C767::AID-PS198%3E3.0.CO;2-Q)
6 445
7

8 446 Trapp, S., 2004. Plant uptake and transport models for neutral and ionic chemicals. Environ. Sci. Pollut.
9 447 Res. 11, 33-39. <https://doi.org/10.1065/espr2003.08.169>
10

11 448 Villeneuve, D.L., Coady, K., Escher, B.I., Mihaich, E., Murphy, C.A., Schlekat, T., Garcia-Reyero, N.,
12 449 2019. High-throughput screening and environmental risk assessment: State of the science and emerging
13 450 applications. Environ. Toxicol. Chem. 38(1), 12-26. <https://doi.org/10.1002/etc.4315>
14

15 451 Wade, C., Glynn, K., 2020. Hands-On Gradient Boosting with XGBoost and scikit-learn: Perform 452
16 accessible machine learning and extreme gradient boosting with Python. Packt Publishing Ltd., 453
17 Birmingham, UK.
18

19 454 Wen, B., Wu, Y., Zhang, H., Liu, Y., Hu, X., Huang, H., Zhang, S., 2016. The roles of protein and lipid in
20 455 the accumulation and distribution of perfluorooctane sulfonate (PFOS) and perfluorooctanoate (PFOA) 456
21 in plants grown in biosolids-amended soils. Environ. Pollut. 216, 682-688.
22 457 <https://doi.org/10.1016/j.envpol.2016.06.032>
23

24 458 Xiang, L., Qiu, J., Chen, Q.-Q., Yu, P.-F., Liu, B.-L., Zhao, H.-M., Li, Y.-W., Feng, N.-X., Cai, Q.-Y., Mo,
25 459 C.-H., 2023. Development, Evaluation, and Application of Machine Learning Models for Accurate 460
26 Prediction of Root Uptake of Per-and Polyfluoroalkyl Substances. Environ. Sci. Technol. 461
27 <https://doi.org/10.1021/acs.est.2c09788>
28

29 462 Zhong, S., Zhang, K., Bagheri, M., Burken, J.G., Gu, A., Li, B., Ma, X., Marrone, B.L., Ren, Z.J., Schrier,
30 463 J., 2021. Machine learning: new ideas and tools in environmental science and engineering. Environ. Sci. 464
31 Technol. 55(19), 12741-12754. <https://doi.org/10.1021/acs.est.1c01339>
32

33 465 Zhu, H., Akroud, M., Zheng, B., Pelegris, A., Jayarajan, A., Phanishayee, A., Schroeder, B., Pekhimenko,
34 466 G., 2018. Benchmarking and analyzing deep neural network training, 2018 IEEE Int. Symp. Workload 467
35 Charact. IEEE, pp. 88-100. <https://doi.org/10.1109/IISWC.2018.8573476>
36

37 468 Zhu, W., Webb, Z.T., Mao, K., Romagnoli, J., 2019. A deep learning approach for process data visualization
38 469 using t-distributed stochastic neighbor embedding. Ind. Eng. Chem. Res. 58(22), 9564-9575. 470
39 <https://doi.org/10.1021/acs.iecr.9b00975>

40 471 Zien, A., Krämer, N., Sonnenburg, S., Rätsch, G., 2009. The feature importance ranking measure, Machine
41 472 Learning and Knowledge Discovery in Databases: European Conference, ECML PKDD 2009, Bled, 473
42 Slovenia, September 7-11, 2009, Proceedings, Part II 20. Springer, pp. 694-709.
43 474 https://doi.org/10.1007/978-3-642-04174-7_45
44
45 475
46
47 476
48
49 477
50
51 478
52
53 479
54
55 480
56
57 481
58
59 482
60
61 483
62
63
64
65

1
2
3
4 484 Lists of figure captions:
5
6 485 Fig. 1. Architecture of the deep neural networks with eleven inputs for predicting TSCF and RCF.
7
8 486 Fig. 2. Visualization of the hidden patterns in the TSCF and RCF data sets using t-SNE.
9
10 487 Fig. 3. Significance of different predictive variables for the TSCF and RCF models based on
11 488 feature importance analysis using XGBoost.
12
13 489 Fig. 4. Performance of the deep learning models for the TSCF based on test data. Regression plots
14 490 and training history for the deep neural networks (A1 and A2), recurrent neural networks (B1 and
15 491 B2), and long short-term memory (C1 and C2).
16
17 492 Fig. 5. Performance of the deep learning models for the RCF based on test data. Regression plots
18 493 and training history for the deep neural networks (A1 and A2), recurrent neural networks (B1 and
19 494 B2), and long short-term memory (C1 and C2).
20
21 495 Fig. 6. Relationships between lipid and protein contents in plant roots and RCFs of emerging
22 496 contaminants.
23
24 497
25
26 498
27
28 499
29
30
31
32
33
34
35
36
37
38
39
40
41
42
43
44
45
46
47
48
49
50
51
52
53
54
55
56
57
58
59
60
61
62
63
64
65

Table 1 Characteristics of the parameters used in the deep learning modeling processes.

Input parameter	Minimum		Output parameter	Min-Max
	TSCF	RCF		
log K _{ow}	-2.19–6.75	-0.88–8.15	TSCF	0.001–1.16
MW (Da)	32–616.4	52–765	RCF	0.009–497.15
HBD	0–6	0–5	log RCF	-2.046–2.696
HBA	0–16	0–11		
RB	0–36	0–13		
PSA (A ²)	0–196.2	0–161		
VP (mm Hg)	4.6e-18–538	0–167		
HL (day)	0.5–832	3–832		
WS (mg/L)	2.0e-4–1.0e-6	2.0e-4–1.0e-6		
Root lipids (%)	0.1–7.2	0.16–9		
Root proteins (%)	1.35–23	1.35–28		

Table 2 Predictive performance of the three deep learning models compared to the reported studies.

Model	Input	Output	R ²	Error	Reference
RNN DNN LSTM	Nine chemical and two plant root properties	log RCF	0.91	MSE = 0.071	This study
			0.90	MSE = 0.124	
			0.84	MSE = 0.126	
RNN DNN LSTM	Nine chemical and two plant root properties	TSCF	0.67	MSE = 0.035	This study
			0.62	MSE = 0.055	
			0.56	MSE = 0.060	
ANN	Six physicochemical properties	TSCF	0.54	MSE = 0.037	Bagheri et al. (2019)
ANN	Six physicochemical properties	RCF	0.80	MSE = 922.2	Bagheri et al. (2020)
GBRT RF FCNN SVR	Molecular, soil, and root properties	log RCF	0.76	MAE = 0.23	Gao et al. (2022)
			0.71	MAE = 0.25	
			0.79	MAE = 0.22	
			0.68	MAE = 0.26	
BPNN	Three physicochemical and soil properties	RCF	0.80	-	Wang et al. (2021)

RNN: Recurrent neural networks, DNN: Deep neural networks, LSTM: Long short-term memory, ANN: Artificial neural networks, GBRT: Gradient boosted regression trees, RF: Random forest, FCNN: Fully connected neural networks, SVR: Support vector regression, BPNN: Backpropagation neural networks.

